The Plant Cell, Vol. 25: 1093–1107, March 2013, www.plantcell.org

PROTEIN S-ACYL TRANSFERASE10 Is Critical for Development and Salt Tolerance in *Arabidopsis*[W]

Liang-Zi Zhou,[a,1] Sha Li,[a,1] Qiang-Nan Feng,[a] Yu-Ling Zhang,[a] Xinying Zhao,[a] Yong-lun Zeng,[b] Hao Wang,[b] Liwen Jiang,[b] and Yan Zhang[a,2]

[a] State Key Laboratory of Crop Biology, Shandong Agricultural University, Tai'an 271018, Shandong, China
[b] School of Life Sciences, Centre for Cell and Developmental Biology, The Chinese University of Hong Kong, Hong Kong 999077, China

Protein *S*-acylation, commonly known as palmitoylation, is a reversible posttranslational modification that catalyzes the addition of a saturated lipid group, often palmitate, to the sulfhydryl group of a Cys. Palmitoylation regulates enzyme activity, protein stability, subcellular localization, and intracellular sorting. Many plant proteins are palmitoylated. However, little is known about protein *S*-acyl transferases (PATs), which catalyze palmitoylation. Here, we report that the tonoplast-localized PAT10 is critical for development and salt tolerance in *Arabidopsis thaliana*. *PAT10* loss of function resulted in pleiotropic growth defects, including smaller leaves, dwarfism, and sterility. In addition, *pat10* mutants are hypersensitive to salt stresses. We further show that PAT10 regulates the tonoplast localization of several calcineurin B–like proteins (CBLs), including CBL2, CBL3, and CBL6, whose membrane association also depends on palmitoylation. Introducing a C192S mutation within the highly conserved catalytic motif of PAT10 failed to complement *pat10* mutants, indicating that PAT10 functions through protein palmitoylation. We propose that PAT10-mediated palmitoylation is critical for vacuolar function by regulating membrane association or the activities of tonoplast proteins.

INTRODUCTION

S-acylation is a eukaryotically conserved, reversible posttranslational modification catalyzing the addition of a saturated acyl group to the sulfhydryl group of a Cys to form a thioester (Baekkeskov and Kanaani, 2009; Greaves and Chamberlain, 2011). The 16-carbon palmitate is the most common fatty acid added through *S*-acylation in animals (Greaves and Chamberlain, 2011), although other lipids with different chain lengths, such as stearate, are often added in plants (Sorek et al., 2007; Batistic et al., 2008). Historically and adopted hereafter, palmitoylation is used to refer to *S*-acylation. Palmitoylation regulates membrane association of soluble proteins, partitioning of transmembrane proteins into lipid rafts, protein activity, protein trafficking into different membrane compartments, as well as protein stability and turnover (Hemsley and Grierson, 2008; Baekkeskov and Kanaani, 2009; Greaves and Chamberlain, 2011). In yeast and animals, proteins subject to palmitoylation, such as transmembrane receptors, small GTPases, and Ca^{2+} sensors, usually play critical roles in cell signaling. Furthermore, proteomic studies in yeast and animal cells showed that a large number of proteins are palmitoylated (Roth et al., 2006; Kang et al., 2008), implying that palmitoylation may play more important roles in eukaryotic cells than currently appreciated.

Despite a long period of doubt on whether palmitoylation necessitates specific enzymes, there are three types of protein *S*-acyl transferases currently known to catalyze palmitoylation, including membrane-bound *O*-acyltransferases, longin domain proteins and Asp-His-His-Cys motif Cys-rich domain (DHHC-CRD) protein *S*-acyl transferases (PATs) (Greaves and Chamberlain, 2011), among which the DHHC-CRD–type PATs are the most well studied. *PAT*s are present in all eukaryotic genomes as relatively large families, including seven in yeast, 23 in human, and 24 in *Arabidopsis thaliana* (Hemsley et al., 2005; Greaves and Chamberlain, 2011; Batistic, 2012). PATs typically contain four to six transmembrane domains and the highly conserved DHHC catalytic domain (Hemsley et al., 2005; Hemsley and Grierson, 2008; Greaves and Chamberlain, 2011; Batistic, 2012). Each eukaryotic genome additionally encodes one to two PATs with ankyrin repeat domains (Hemsley et al., 2005; Hemsley and Grierson, 2008; Greaves and Chamberlain, 2011; Batistic, 2012).

An increasing number of plant proteins are found to be regulated by palmitoylation. Palmitoylation regulates membrane anchoring of small GTPase ARA6 (Ueda et al., 2001), protein phosphatases (Gagne and Clark, 2010), heterotrimeric G protein subunits (Zeng et al., 2007), and a few calcium sensors (Martín and Busconi, 2000; Batistic and Kudla, 2009; Batistič et al., 2012). Palmitoylation also regulates microdomain partitioning and possibly subcellular trafficking of Rho of plants (ROP GTPases) (Sorek et al., 2007, 2010). A recent proteomic analysis using *Arabidopsis* root cell culture identified over 500 proteins to be putatively *S*-acylated (Hemsley et al., 2013), thus establishing palmitoylation as an important posttranslational modification in plants. Palmitoylated proteins play diverse roles in plant cells, including development (Gagne and Clark, 2010), vesicle trafficking (Ueda et al., 2001), cell

[1] These authors contributed equally to this work.
[2] Address correspondence to yzhang@sdau.edu.cn.
The author responsible for distribution of materials integral to the findings presented in this article in accordance with the policy described in the Instructions for Authors (www.plantcell.org) is: Yan Zhang (yzhang@sdau.edu.cn).
[W] Online version contains Web-only data.
www.plantcell.org/cgi/doi/10.1105/tpc.112.108829

morphogenesis (Sorek et al., 2010), and abiotic stress responses (Batistič et al., 2012).

Despite the importance of palmitoylation in plants (Hemsley and Grierson, 2008), progress in understanding the enzymes catalyzing protein palmitoylation has been slow. *Arabidopsis TIP GROWTH DEFECTIVE1* (*TIP1*) is the only plant *PAT* with characterized function to date. *TIP1* loss of function resulted in defective growth of pollen tubes and root hairs (Hemsley et al., 2005). In contrast with *TIP1*, which encodes an *Arabidopsis* PAT with the ankyrin domains, functional analysis of other *PAT*s by reverse genetics was considered problematic due to potential functional redundancy (Hemsley and Grierson, 2008) implied by their similar domain organization and overlapping expression patterns (Zimmermann et al., 2004). However, *PAT*s encode transmembrane proteins whose functional specificity is not only determined by their expression patterns but also by their residential membrane compartments (Greaves and Chamberlain, 2011). Indeed, global analysis of yeast and mammalian PATs showed that PATs of a given species could localize at various membrane compartments, including endoplasmic reticulum, Golgi apparatus, plasma membrane, secretory vesicles, and vacuole (Ohno et al., 2006). A recent study using transient expression assays in tobacco (*Nicotiana tabacum*) showed that *Arabidopsis* PATs were also localized at different membrane compartments (Batistic, 2012).

We report here functional analysis of *PAT10* in *Arabidopsis*. *PAT10* is constitutively expressed. Functional loss of *PAT10* resulted in pleiotropic developmental defects, including reduced vegetative and reproductive growth, sporophytic and gametophytic male defects, and compromised ability of pistils to support pollen tube growth. Both cell expansion and cell division were reduced in *pat10*. Using stable transgenic plants for fluorescent colabeling, we showed that PAT10 localizes at vacuolar membrane (i.e., the tonoplast) but not at Golgi or any post-Golgi vesicles. In addition to the developmental defects, mutants of *PAT10* were hypersensitive to salt stresses. We further identified a subfamily of calcineurin B–like proteins (CBLs) as putative substrates of PAT10. Localization of CBL2, CBL3, and CBL6 at the tonoplast depended on functional PAT10. Our results demonstrate that PAT10-mediated protein palmitoylation at the tonoplast is critical for development and salt tolerance in *Arabidopsis*.

RESULTS

Characterization of *PAT10* Loss-of-Function Mutants

We used a reverse genetic approach to understand the function of *Arabidopsis* PATs and identified two T-DNA insertion lines for *PAT10*. T-DNA was inserted at the 10th intron or the 10th exon of *PAT10* genomic sequence for *pat10-1* (SALK_024964) and *pat10-2* (WiscDsLox289_292E10), respectively. By PCR analysis, we confirmed that the genomic sequences upstream and downstream of the insertion sites were intact in mutants. To find out whether the T-DNA insertions disrupted *PAT10* expression, we performed RT-PCR analysis on RNAs isolated from seedlings of the wild type and *pat10* mutants. RT-PCRs with a primer pair that amplified upstream sequences of T-DNA insertions detected *PAT10* transcript in both the wild type and *pat10*. However, no transcript was detected in *pat10* mutants when primer pairs flanking the T-DNA insertion sites were used (Figures 1A and 1B), suggesting that *pat10* mutants were not able to produce full-length *PAT10*. Experiments using both *pat10-1* and *pat10-2* produced identical results. Therefore, results reported hereafter were those obtained with *pat10-1* unless noted.

Homozygous *pat10* mutants displayed pleiotropic developmental defects compared with the wild type under soil growth condition. *pat10* was substantially smaller and developed more slowly. As a result, growth differences became more pronounced over time.

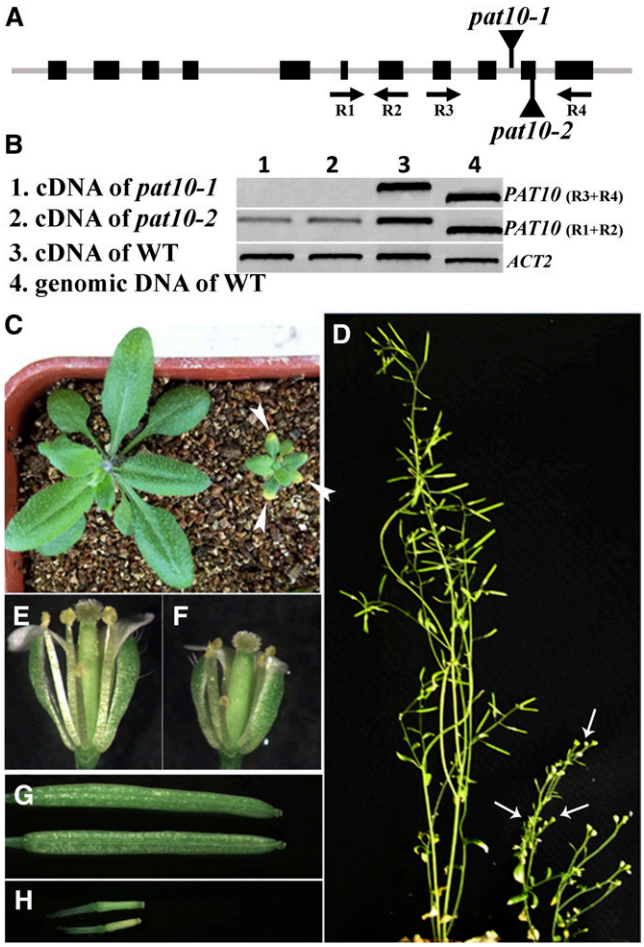

Figure 1. Mutations at *PAT10* Caused Pleiotropic Developmental Defects.

(A) Schematic illustration of T-DNA insertions within the *PAT10* genomic region.
(B) RT-PCR analysis showing that *pat10* mutants are devoid of full-length *PAT10* transcripts. WT, the wild type.
(C) A representative image of the wild type (left) and *pat10* (right) at 20 DAG. Arrowheads indicate necrotic leaf tips in the mutant plant.
(D) A representative image of the wild type (left) and *pat10* (right) at 50 DAG. Arrows point to nonelongated siliques.
(E) A representative image of wild-type open flowers.
(F) A representative image of *pat10* open flowers.
(G) Fully elongated siliques in the wild type.
(H) Nonelongated siliques in *pat10*.

Rosette leaves of *pat10* were much smaller than those of the wild type at 20 d after germination (DAG) (Figure 1C), although leaf shape was normal (Figure 1C). The size reduction was due to reduced cell number as well as reduced cell expansion (see Supplemental Figure 1 online). In addition, *pat10* showed early senescence on the leaf tips when growing in soil at 20 DAG (Figure 1C). During floral transition, *pat10* showed no correlation between flowering time and rosette leaf number such that they flowered temporally later but had fewer rosette leaves than the wild type (see Supplemental Figure 2 online), likely a consequence of slow development. Inflorescence stems were much shorter for *pat10* than for the wild type (Figure 1D). Mutant flowers (Figure 1F) were also smaller than those of the wild type (Figure 1E). Although stamen filaments of *pat10* were shorter than the wild type, pistils of *pat10* mutants were also shorter (Figures 1E and 1F), allowing reaching of stigma surface by pollen. *pat10* growing in soil were completely sterile (Figure 1D) without elongating siliques (Figure 1H).

Sporophytic and Gametophytic Male Defects in *pat10*

Although we were able to obtain homozygous *pat10* mutants from self-pollinated heterozygous *pat10*, the ratio of homozygous to heterozygous mutants was much lower than expected (Table 1). This suggested that the loss of *PAT10* led to gametophytic defects. To find out which gametophyte was defective due to *PAT10* loss of function, we performed reciprocal crosses between heterozygous *pat10* mutants and the wild type. Results showed that pollen of *pat10* did not transmit as well as that of the wild type, while female gametophytes were not affected (Table 1). These results suggested that the defective male gametophytes were caused by *PAT10* loss of function.

To find out at which stage male gametophytes of *pat10* was defective, we next analyzed pollen viability using 4',6-diamidino-2-phenylindole and Alexander's stain. No differences were observed regarding pollen viability between the wild type and *pat10* (see Supplemental Figure 3 online), suggesting that *PAT10* did not regulate pollen viability. However, scanning electron microscopy (SEM) showed that the deposition of the pollen coat was abnormal in homozygous *pat10* mutants (Figures 2C and 2F), even though no difference was observed in the pollen coats of heterozygous *pat10* plants (Figures 2B and 2E) versus in the wild type (Figures 2A and 2D). Because deposition of the pollen coat depends on the sporophytic tapetum, we concluded that *PAT10* loss of function also caused sporophytic male defects. Transmission electron microscopy (TEM) further confirmed the pollen coat defect of *pat10* (Figure 2J), whereas *pat10* pollen contained fewer lipid bodies (Figure 2L) than the wild type (Figure 2I).

We further analyzed in vitro pollen germination and growth. A low percentage of *pat10* pollen germinated (Figures 3A and 3B). Pollen germination of heterozygous *pat10* was also significantly reduced compared with the wild type (Figures 3A and 3B), suggesting that mutations at *PAT10* not only caused sporophytic male defects but also affected gametophytic male function. Mutant pollen tubes ceased growth early, resulting in short tubes (Figures 3A and 3C).

To find out whether *PAT10* regulated pollen tube growth in vivo, we performed aniline blue staining on emasculated wild-type pistils hand-pollinated with pollen either from the wild type or *pat10*. At 9 h after pollination (HAP) when most wild-type pollen tubes reached to the bottom of a pistil (Figure 3D), pollen tubes of *pat10* just emerged from the style (Figure 3E). At 48 HAP, all ovules in pistils pollinated by the wild type were fertilized and developing (Figure 3F). By contrast, few ovules were targeted by *pat10* pollen tubes at 48 HAP despite the fact that the mutant pollen tubes had reached the bottom of the pistils (Figure 3G). These results suggested that polar and directional growth of pollen tubes was compromised by *PAT10* loss of function.

Sporophytic Female Defects by *PAT10* Loss of Function

Our reciprocal analysis using the wild type and heterozygous *pat10* mutants indicated that female gametophytes were not affected by *PAT10* loss of function. However, reciprocal crosses using wild-type pollen and *pat10* pistils failed to produce seeds. To find out whether *PAT10* loss of function caused sporophytic female defects, we performed aniline blue staining on *pat10* pistils pollinated with wild-type pollen. At 24 HAP, when wild-type pollen tubes reached to the bottom of wild-type pistils (Figure 4A), they hardly reached to the middle of *pat10* pistils (Figure 4B), suggesting that *pat10* pistils could not support pollen tube growth. SEM analysis of mature ovules did not reveal morphological differences

Table 1. Loss of Function of *PAT10* Resulted in Defective Male Transmission

Experiment Parent	F1 Segregation		
Female × Male	Genotype	Expected Ratio	Observed
1. *pat10-1*+/− × wild type	*PAT10*+/+: +/−	1:1	90:98[a]
2. Wild type × *pat10-1*+/−	*PAT10*+/+: +/−	1:1	121:7[b]
3. *pat10-2*+/− × wild type	*PAT10*+/+: +/−	1:1	96:71[a]
4. Wild type × *pat10-2*+/−	*PAT10*+/+: +/−	1:1	160:55[b]
5. *pat10-1*+/− × *pat10-1*+/−	*PAT10*+/+:+/−:−/−	1:2:1	115:208:50[c]
6. *pat10-2*+/− × *pat10-2*+/−	R:S[d]	3:1	507:228[e]

[a]Not significantly different from the segregation ratio 1:1 (Student's *t* test, $P > 0.05$).
[b]Significantly different from the segregation ratio 1:1 (Student's *t* test, $P < 0.01$).
[c]Significantly different from the segregation ratio 1:2:1 (Student's *t* test, $P < 0.01$).
[d]R for Basta resistant and S for Basta sensitive. The mutant copy of *pat10-2* is resistant to Basta salt; therefore, Basta resistance was calculated here.
[e]Significantly different from the segregation ratio 3:1 (Student's *t* test, $P < 0.01$).

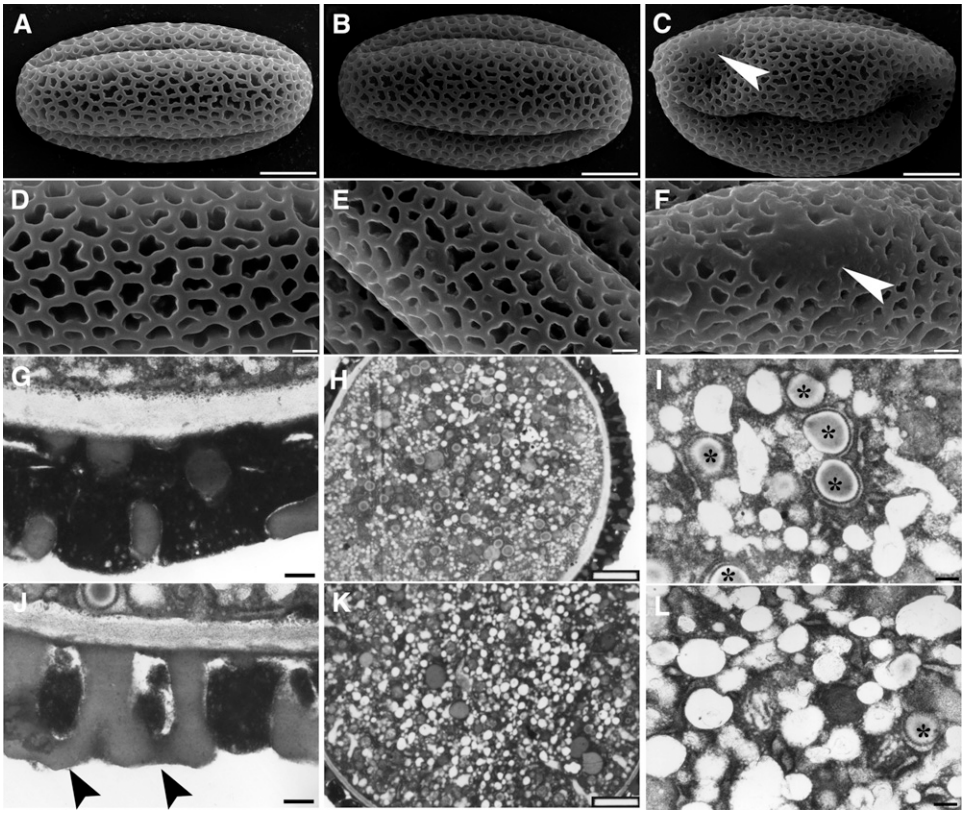

Figure 2. Mutations at *PAT10* Caused Pollen Developmental Defects.

(A) to **(C)** Scanning electron micrographs (SEM) of mature pollen from the wild type **(A)**, heterozygous *pat10* mutants **(B)**, and homozygous *pat10* mutants **(C)**. Arrowhead indicates defective pollen coat.
(D) to **(F)** Close-ups of SEM images shown in **(A)** to **(C)**, respectively. Arrowhead indicates defective pollen coat.
(G) and **(J)** Transmission electron micrograph (TEM) of mature pollen from the wild type **(G)** and *pat10* **(J)** showing pollen coat structure. Arrowheads indicate defective pollen coats.
(H) and **(K)** TEM section of mature pollen from the wild type **(H)** and *pat10* **(K)**.
(I) and **(L)** Close-ups of TEM shown in **(H)** and **(K)**, respectively. Asterisks indicate lipid bodies.
Bars = 5 μm in **(A)** to **(C)**, 1 μm in **(D)** to **(F)**, 2 μm in **(H)** and **(K)**, and 200 nm in **(G)**, **(I)**, **(J)**, and **(L)**.

between the wild type (Figure 4C) and *pat10* (Figure 4D) regarding ovule integuments. We further performed optical sections on unfertilized mature ovules as well as ovules immediately after fertilization. Interestingly, embryo sacs of *pat10* were found to be disorganized at the chalazal end (Figure 4I) compared with the ordered organization in the wild type (Figure 4E). In contrast with normal embryo development in the wild type after fertilization (Figures 4F to 4H), embryo sacs of *pat10* gradually degenerated likely due to fertilization failure (Figures 4J to 4L). No such embryo sac defects were observed in ovules from heterozygous *pat10* mutants (see Supplemental Figure 4 online), which correlated with the normal transmission of mutant female gametophytes during reciprocal crosses (Table 1).

Constitutive Expression of *PAT10*

The pleiotropic developmental defects by *PAT10* loss of function suggested a constitutive expression pattern. Indeed, *PAT10* was previously found to be expressed in all tissues via microarray analysis (Zimmermann et al., 2004). In addition, we analyzed the expression pattern of *PAT10* using Pro_{PAT10}:GUS (for β-glucuronidase) reporter lines by histochemical analysis. GUS signals were detected in mature embryos, cotyledons, and whole seedlings (Figures 5A, 5B, and 5D). In mature leaves, the GUS signal was highest at hydathodes as well as in guard cells (Figure 5C). *PAT10* was strongly expressed at the sites of lateral root initiation and at root tips (Figure 5E). Dissection of GUS signals in vascular bundles showed that *PAT10* was expressed strongly in phloem but not in xylem (Figures 5F and 5G).

It is intriguing that the GUS signal was not detected at most reproductive tissues (Figure 5H), whereas *PAT10* loss of function resulted in developmental defects. We reasoned that the promoter sequences used to generate Pro_{PAT10}:GUS reporter lines might not contain all of the information required for expression. Therefore, we next performed RNA in situ hybridization to find out whether *PAT10* was expressed in reproductive tissues. Indeed, *PAT10* was strongly expressed in the tapetal layer of developing anthers starting from anther developmental stage

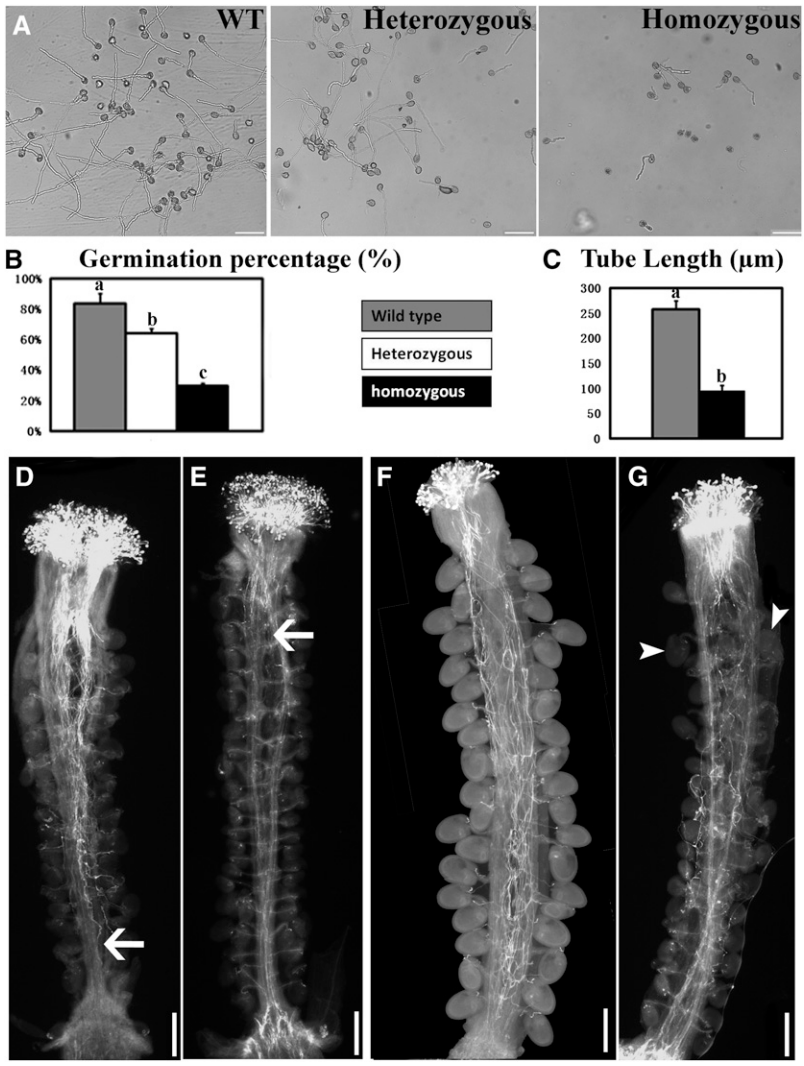

Figure 3. *PAT10* Mutations Resulted in Defective Pollen Germination and Tube Growth.

(A) In vitro germination of pollen from the wild type (WT), heterozygous *pat10* mutants (heterozygous), and homozygous *pat10* mutants (homozygous).

(B) In vitro germination percentage of the wild type, heterozygous *pat10* mutants, and homozygous *pat10* mutants. Germination percentage was calculated from three independent experiments, including around 400 pollen grains in each experiment. For each experiment, samples from three genetic backgrounds were placed side by side on the same slide to reduce system variations. Results are given as means ± SE. Samples with different letters (a, b, and c) are significantly different from each other by Fisher's LSD method.

(C) Tube length of in vitro grown pollen from the wild type and *pat10*. Data were collected from three independent experiments, each including 80 to 100 pollen tubes. For each experiment, samples from the two genetic backgrounds were placed side by side on the same slides to reduce system variations. Results are given as means ± SE. Samples with different letters (a and b) are significantly different from each other by Fisher's LSD method.

(D) and **(E)** Aniline blue staining of emasculated wild-type pistils hand-pollinated with wild-type pollen **(D)** or with *pat10* pollen **(E)** at 9 HAP. Arrows point to the growth fronts of pollen tubes.

(F) and **(G)** Aniline blue staining of emasculated wild-type pistils hand-pollinated with wild-type pollen **(F)** or *pat10* pollen **(G)** at 48 HAP. Arrowheads point to ovules fertilized by *pat10* pollen.

Bars = 100 μm in **(A)** and 200 μm in **(D)** to **(G)**.

6 (Figures 6A and 6B). With tapetal degeneration, *PAT10* expression gradually increased in developing microspores (Figures 6C and 6D) and in mature pollen (Figures 6E and 6F). *PAT10* was also expressed at the embryo sacs and surrounding cells in mature pistils (Figures 6G and 6H). In addition, no signal was detected in reproductive organs when identical RNA in situ hybridization was performed in *pat10* (see Supplemental Figure 5 online), indicating that the probe was specific for *PAT10* without cross-reacting with the other 23 PATs (Hemsley and Grierson, 2008; Batistic, 2012).

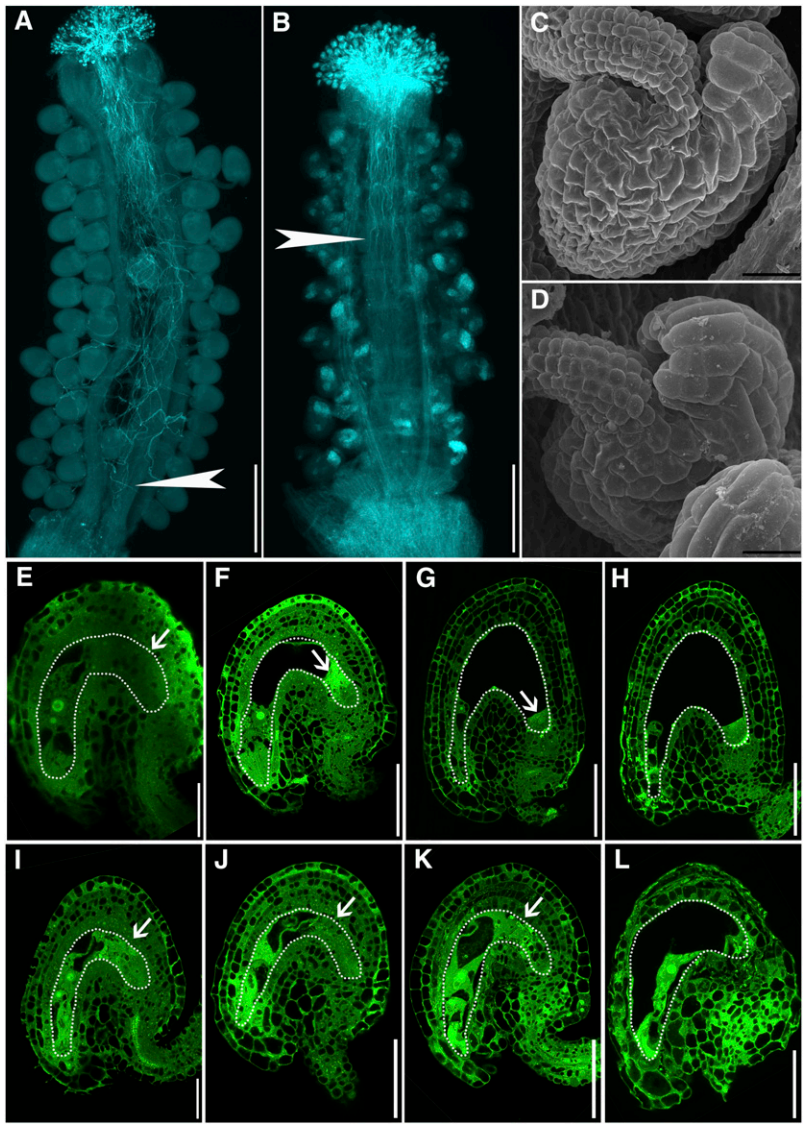

Figure 4. Female Reproductive Organs Are Defective in *pat10*.

(A) and **(B)** Aniline blue staining of emasculated wild-type pistils **(A)** and *pat10* pistils **(B)** hand-pollinated with wild-type pollen at 24 HAP. Arrows indicate the growth fronts of pollen tubes.
(C) and **(D)** Scanning electron microscopy of a mature ovule from the wild type **(C)** and *pat10* **(D)**.
(E) to **(H)** Optical sections of wild-type ovules from unfertilized mature pistils **(E)** and from pistils at 9 HAP **(F)**, 24 HAP **(G)**, and 48 HAP **(H)**. Dotted lines highlight the embryo sacs. Arrows indicate the chalazal end.
(I) to **(L)** Optical sections of *pat10* ovules from unfertilized mature pistils **(I)** and from pistils at 9 HAP **(J)**, 24 HAP **(K)**, and 48 HAP **(L)**. Dotted lines highlight the embryo sacs. Arrows indicate the chalazal end.
Bars = 200 μm in **(A)** and **(B)**, 20 μm in **(C)** and **(D)**, 25 μm in **(E)** and **(I)**, and 50 μm in **(F)** to **(H)** and **(J)** to **(L)**.

PAT10 but Not $PAT10_{C192S}$ Complemented *pat10*

To confirm that the pleiotropic developmental defects were caused by *PAT10* loss of function, we performed a complementation study in which we introduced a *PAT10* genomic fragment green fluorescent protein (GFP) translational fusion (*PAT10-GFP*) into *pat10*. Exogenous *PAT10* expression rescued all defects of the *pat10* mutants (see Supplemental Figure 6 online), confirming the null mutant identity of *pat10*. Since the GFP translational fusion did not interfere with the function of PAT10, we therefore used it to study the subcellular localization of PAT10 by fluorescence microscopy. Unlike the Pro_{PAT10}:GUS reporter lines, which showed no signal in most reproductive tissues, the GFP signal was detected in pollen (see Supplemental Figure 7 online), confirming that *PAT10* expression in reproductive tissues or cells requires intronic sequences.

Because animal PATs can have functions independent of their enzymatic activities (Greaves and Chamberlain, 2011), we wondered whether *Arabidopsis* PAT10 regulated development

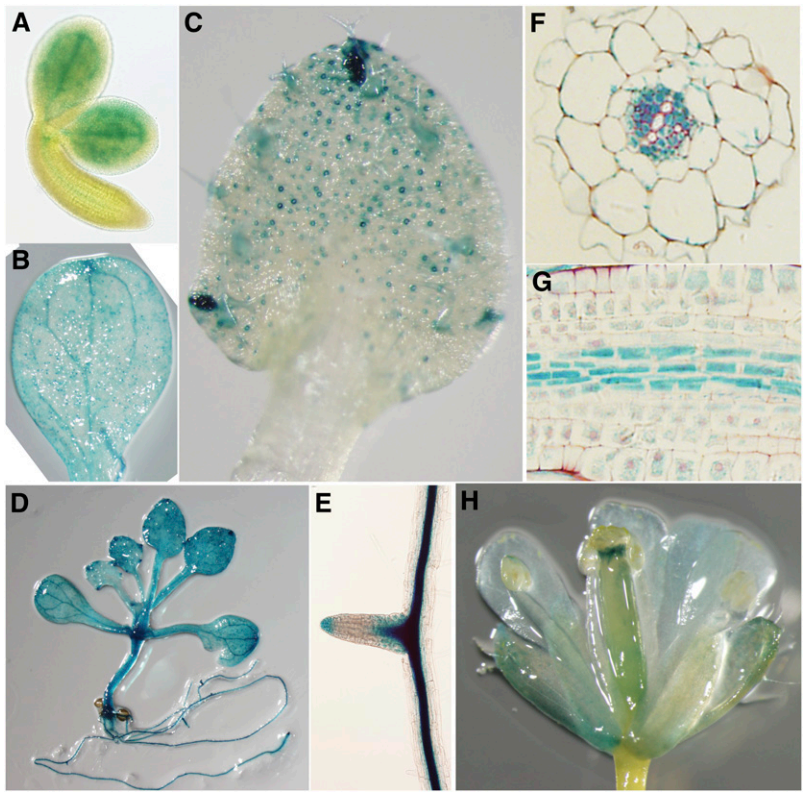

Figure 5. Constitutive Expression of *PAT10* by Pro_{PAT10}:GUS Reporter Analysis.

(A) A mature embryo freshly dissected from rehydrated mature seeds.
(B) A cotyledon showing GUS signals at vascular tissues.
(C) A true leaf showing strong GUS signals at hydathodes, trichomes, and guard cells.
(D) A seedling at 15 DAG showing constitutive GUS signals at both aerial parts and in roots.
(E) A lateral root.
(F) A transverse section of Pro_{PAT10}:GUS transgenic roots showing strong GUS signal at the phloem but not at the xylem.
(G) A longitudinal section of Pro_{PAT10}:GUS transgenic roots showing strong GUS signal at the vascular bundles.
(H) An open flower of a Pro_{PAT10}:GUS transgenic plant showing strong GUS signal at the style and stomata of floral organs.

through its *S*-acyl transferase activity. Therefore, we introduced a point mutation at *PAT10* so that the conserved DHHC motif was changed to DHHS ($PAT10_{C192S}$), as such a mutation was previously shown to abolish PAT activity (Hemsley et al., 2005; Baekkeskov and Kanaani, 2009; Greaves and Chamberlain, 2011). The exogenous $PAT10_{C192S}$-*GFP* did not rescue *pat10* (see Supplemental Figure 8 online), suggesting that PAT10 functions through its palmitate transferase activity.

PAT10 Is Localized at the Tonoplast

The subcellular localization of *Arabidopsis* PATs was recently performed via transient expression in *Nicotiana benthamiana* leaves (Batistic, 2012). When PAT10 was transiently expressed in tobacco epidermal cells, this protein mostly colocalized with a Golgi marker but reached the tonoplast several days later (Batistic, 2012). We introduced the Wave lines expressing red fluorescent protein (RFP)-labeled endomembrane markers (Geldner et al., 2009) into the complemented plants (*PAT10-GFP*;*pat10-1*) for analysis via confocal fluorescence microscopy. PAT10 did not colocalize with the *trans*-Golgi network/early endosome (TGN/EE) marker (Figure 7A) nor the Golgi marker (Figure 7B) or the prevacuolar compartment marker (Figure 7C). Instead, PAT10 showed significantly colocalization with the tonoplast marker WAVE9R (Figure 7D) (Geldner et al., 2009).

We also performed an uptake study in the complemented lines expressing *PAT10-GFP* in *pat10* using the endocytic dye FM4-64 (Lam et al., 2007; Geldner et al., 2009; Bassil et al., 2011a). After 3 h of FM4-64 uptake, the GFP signal completely merged with FM4-64 at the tonoplast (see Supplemental Figure 9 online). Addition of Brefeldin A (BFA), a fungal toxin that interferes with vesicle trafficking at the Golgi and the TGN/EE (Lam et al., 2009), caused aggregation of FM4-64–positive vesicles but not PAT10-labeled compartments.

Since $PAT10_{C192S}$-*GFP* did not rescue *pat10*, we next wanted to find out if the C192S mutation altered its subcellular localization, thus failing to complement. An FM4-64 uptake study was performed in lines expressing $PAT10_{C192S}$-*GFP*. Similar to PAT10-GFP, the majority of $PAT10_{C192S}$-GFP localized at the tonoplast together with FM4-64 after 3 h uptake (see Supplemental Figure 10 online).

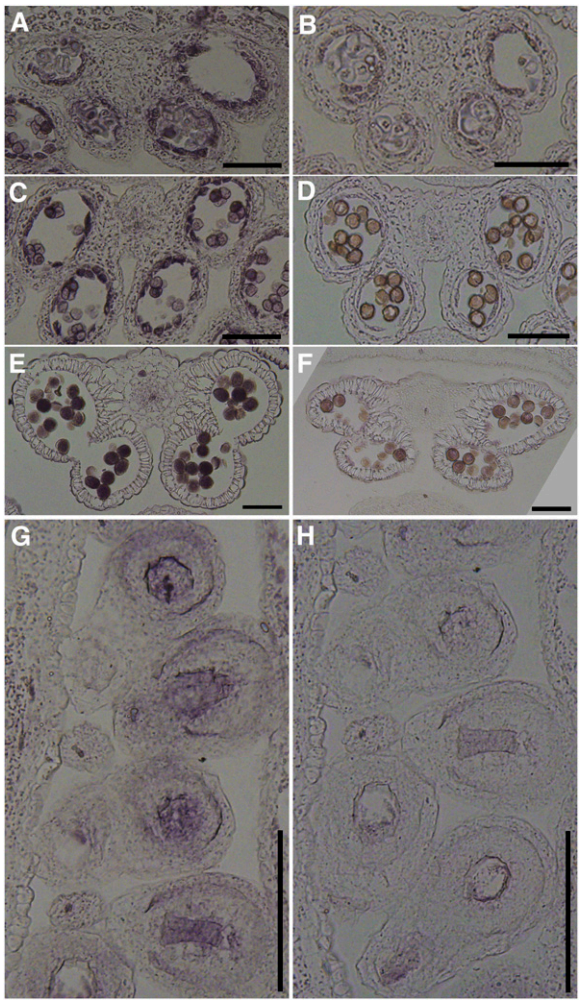

Figure 6. Expression of *PAT10* in Tapetum, Pollen, and Developing Ovules by RNA in Situ Hybridization Analysis.

(A) and **(B)** A stage 6 wild-type anther labeled by the antisense probe **(A)** or the sense probe **(B)**. The tapetal layer shows strong signal.
(C) and **(D)** A stage 9 wild-type anther labeled by the antisense probe **(C)** or the sense probe **(D)**. Strong signal is not only detected at the tapetal layer but also in developing pollen.
(E) and **(F)** A stage 12 wild-type anther labeled by the antisense probe **(E)** or the sense probe **(F)**. The tapetal layer is fully degenerated. Strong signals are present in mature pollen.
(G) and **(H)** Longitudinal sections of unfertilized mature pistils from wild-type plants labeled by the antisense probe **(G)** or the sense probe **(H)**. Strong signals are present at the embryo sacs and its surrounding cells. Bars = 100 μm.

However, in contrast with PAT10 (see Supplemental Figure 9 online), additional punctate vesicles were detected for $PAT10_{C192S}$ (see Supplemental Figure 10 online). Such punctate localization was also detected in pollen tubes expressing $PAT10_{C192S}$ but not in pollen tubes expressing PAT10 (see Supplemental Figure 7 online). Upon BFA treatment, these GFP-labeled vesicles aggregated to regions surrounding the FM4-64–positive BFA compartments (se Supplemental Figure 10 online), indicating that these vesicles were Golgi apparatus (Lam et al., 2009).

PAT10 Loss of Function Caused Hypersensitivity to Salt Stresses

The tonoplast localization of PAT10 prompted us to test the responses of *pat10* to salt and osmotic stresses because vacuoles are critical organelles for plant responses to these abiotic stresses (Apse et al., 2003; Cheng et al., 2005; Kim et al., 2007; Bassil et al., 2011b; Kim and Bassham, 2011; Barragán et al., 2012). We applied various stresses to *pat10*, including high concentrations of NaCl, LiCl, KCl, CsCl, $CaCl_2$, mannitol, and abscisic acid. The *pat10* mutants were hypersensitive to NaCl and LiCl, as *pat10* grew poorly under high NaCl and LiCl stresses (Figures 8A to 8C).

Next, we tested the expression of salt-responsive genes, such as *RESPONSIVE TO DESSICATION 29A* (*RD29A*), *RD20*, *EARLY RESPONSIVE TO DESSICATION10* (*ERD10*), and *RESPONSIVE TO ABA18* (*RAB18*), whose expression was greatly induced by abiotic stresses (Magnan et al., 2008; Ryu et al., 2010; Bassil et al., 2011a). Real-time quantitative RT-PCR (qRT-PCR) analysis

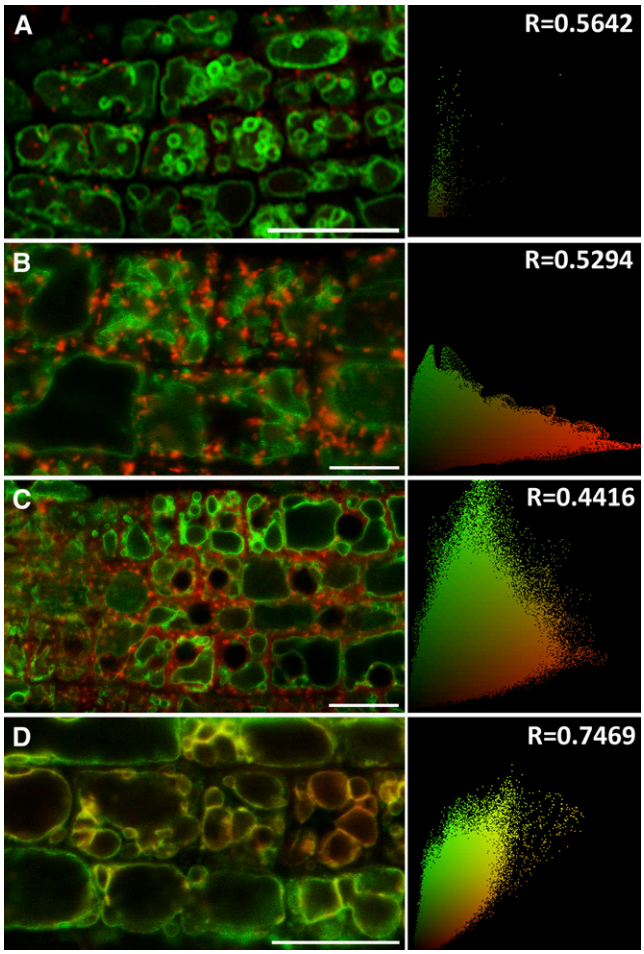

Figure 7. PAT10 Localizes at Tonoplast.

Confocal fluorescence micrographs of transgenic *Arabidopsis* roots coexpressing *PAT10*-GFP (green) and fluorescent markers (red) for the TGN/EE **(A)**, Golgi apparatus **(B)**, the prevacuolar compartments **(C)**, and the tonoplast **(D)**. Pearson's correlation coefficient (R) is shown at the right side of each micrograph. Bars = 10 μm.

showed that salt stresses significantly induced higher expression of *RD29A*, *RD20*, and *ERD10* in *pat10* than in the wild type (Figure 8D). Although the absolute increase of *RAB18* was slightly lower in *pat10* than in the wild type, the induction ratio of *RAB18* in *pat10* was comparable to that of the wild type (Figure 8D). However, *PAT10* itself was not induced by salt stresses (Zimmermann et al., 2004).

Palmitoylation-Regulated Tonoplast Localization of CBL2/3/6 Depended on PAT10

The hypersensitivity of *pat10* to salt stresses gave us a hint about candidate substrates of PAT10. *Arabidopsis* CBLs play critical roles in abiotic stress responses (Batistic and Kudla, 2009; Luan, 2009). Tonoplast localization of CBL2 is regulated by palmitoylation (Batistic et al., 2008; Batistic and Kudla, 2009; Batistič et al., 2012). In addition, the Cys residues for palmitoylation were conserved among several tonoplast-localized CBLs, such as CBL3 and CBL6, indicating that they are likely modified by palmitoylation. We therefore hypothesized that the tonoplast-localized, palmitoylated CBLs are substrates of PAT10.

To find out whether the palmitoylation-regulated tonoplast localization of CBL2 relies on PAT10, we tested the subcellular localization of GFP-fused CBL2 in wild-type or *pat10* protoplasts. CBL2-GFP expressed in the wild-type protoplasts showed tonoplast

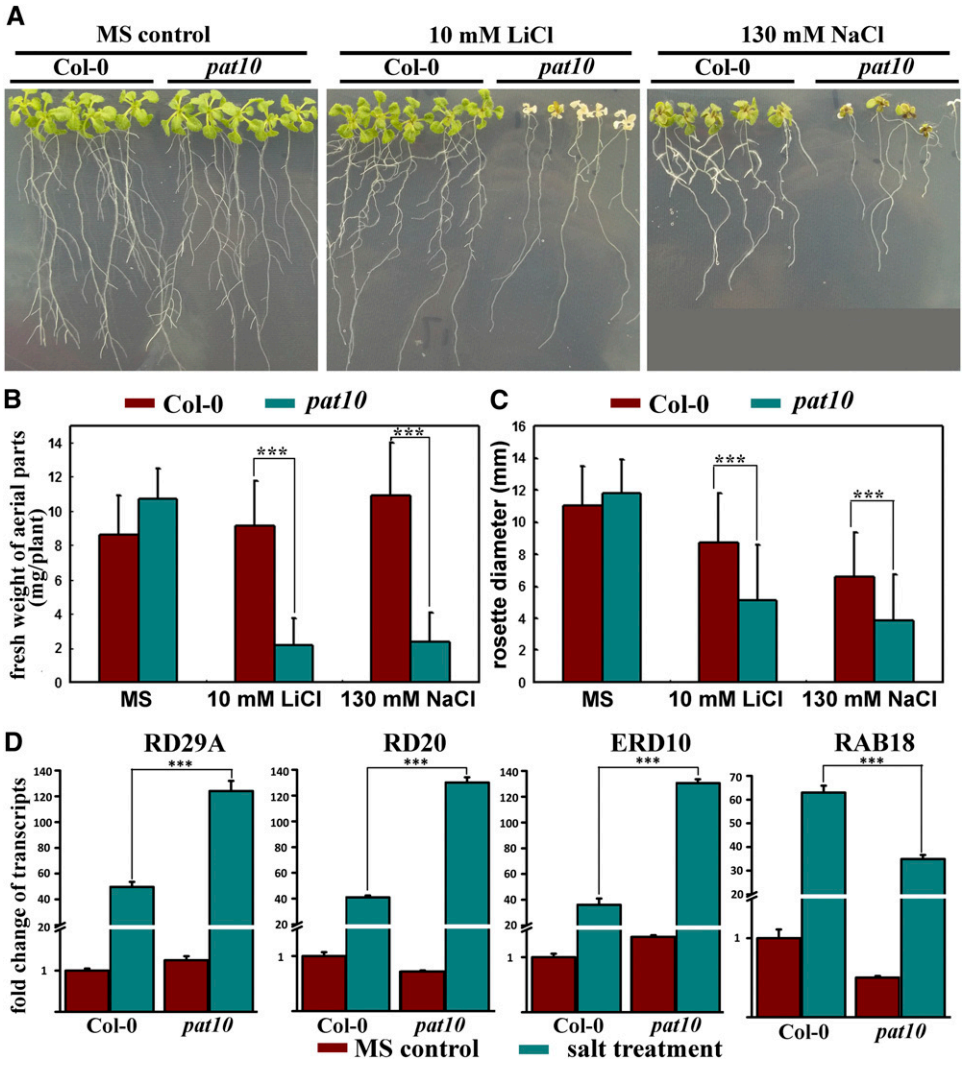

Figure 8. *pat10* Mutants Are Hypersensitive to Salt Stresses.

(A) Seedlings growing either on MS medium, on MS medium supplemented with 10 mM LiCl, or on MS medium supplemented with 130 mM NaCl. Col-0, Columbia-0.

(B) and **(C)** Fresh weight **(B)** and rosette diameter **(C)** of seedlings (aerial parts only) grown on either MS medium, MS medium supplemented with 10 mM LiCl, or MS medium supplemented with 130 mM NaCl. All seedlings were grown on MS for 4 d before being transferred to MS medium or MS supplemented with salts for an additional 14 d. Data were collected from three independent experiments in which at least 30 seedlings were included in each experiment. Results are given as means ± SE. Asterisks indicate significant differences (Student's *t* test, $P < 0.01$).

(D) Induction of salt responsive genes *RD29A*, *RD20*, *ERD10*, and *RAB18* in the wild type or *pat10*. Asterisks indicate significant differences (Student's *t* test, $P < 0.01$).

localization (Figure 9). However, CBL2-GFP expressed in *pat10* was relocated to the cytoplasm (Figure 9), similar to soluble GFP (Figure 9). Because the Cys residues proven to be the palmitoylation sites in CBL2 (Batistič et al., 2012) were also present in CBL3 and CBL6, we suspected that their tonoplast localization was also regulated by PAT10. Indeed, both CBL3 and CBL6 were localized at the tonoplast in wild-type protoplasts, but they became cytosolic in *pat10* protoplasts (Figure 9). Treatment with 2-bromopalmitate (2-BP), a specific inhibitor of protein palmitoylation (Hemsley et al., 2005; Batistič et al., 2012), caused relocalization of CBL2/3/6 from the tonoplast to cytoplasm in wild-type protoplasts (see Supplemental Figure 11 online), confirming their palmitoylation-regulated tonoplast localization. Taken together, these results suggested that CBL2/3/6 are putative substrates of PAT10.

To exclude the possibility that loss of CBL2/3/6 tonoplast localization was caused by a general reduction of cellular palmitoylation owing to *PAT10* loss of function, we introduced CBL9 and ARA6 into *pat10* protoplasts. The plasma membrane–localized CBL9 (Batistic et al., 2010) and the endosome-localized ARA6 (Ueda et al., 2001) both contain sequences for palmitoylation and regulate plant responses to abiotic stresses (Pandey et al., 2004; Ebine et al., 2011). The plasma membrane localization of CBL9 was abolished by 2-BP treatment (see Supplemental Figure 11 online), suggesting that its membrane association depended on palmitoylation. However, membrane association of both CBL9 and ARA6 was retained in *pat10* (see Supplemental Figure 10 online), indicating that *PAT10* loss of function did not reduce protein palmitoylation globally. The membrane localization of ARA7 (a marker for TGN/EE) (Ueda et al., 2001) as well as that of ERD2 (a marker for Golgi apparatus) (Cheung et al., 2002) were not affected by *PAT10* loss of function (Supplemental Figure 12 online), suggesting that the integrity of the endomembrane system was intact.

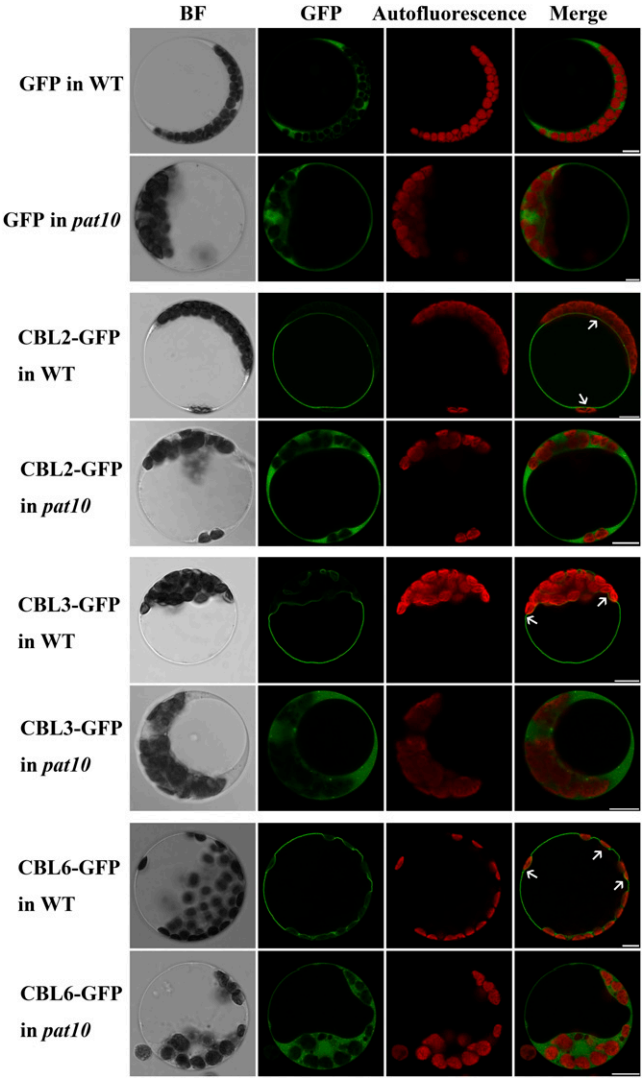

Figure 9. Localization of CBLs at the Tonoplast Depends on Functional PAT10.

Representative images of each treatment (i.e., exogenous expression) are shown. In total, 60 to 80 protoplasts from three independent experiments were visualized for each treatment. BF, bright-field; WT, the wild type. Bars = 10 μm.

DISCUSSION

Arabidopsis PAT10 Regulates Vacuolar Function through Protein Palmitoylation

Plant vacuoles are acidic organelles essential for nutrient remobilization, maintenance of turgor pressure, sequestration of toxic compounds, ions and secondary metabolites, and accumulation of storage proteins (Maeshima, 2001; Mimura et al., 2003; Hamaji et al., 2009; Agee et al., 2010; Krebs et al., 2010; Barragán et al., 2012). Vacuoles occupy ~80 to 90% of the total cell volume and provide cells with the ability to withstand salt and osmotic stresses (Mimura et al., 2003; Hamaji et al., 2009; Barragán et al., 2012). Vacuole function is performed mainly by tonoplast proteins (Maeshima, 2001), including vacuolar H^+-ATPase (Dettmer et al., 2006; Krebs et al., 2010), vacuolar PPase, Ca^{2+}-ATPases (Pittman, 2011), Ca^{2+}/H^+ antiporters (Cheng et al., 2005), K^+ and Na^+/H^+ antiporters (NHXs) (Bassil et al., 2011b; Barragán et al., 2012), tonoplast intrinsic proteins, and CBLs (Kim et al., 2007; Batistic et al., 2010). Functional loss of these tonoplast proteins caused pleiotropic developmental defects and hypersensitivity to abiotic stresses (Apse et al., 2003; Cheng et al., 2005; Batistic et al., 2010; Krebs et al., 2010; Bassil et al., 2011a, 2011b; Barragán et al., 2012), suggesting defective vacuolar function.

In this study, PAT10 was shown to localize at vacuolar membrane. Loss of function of *PAT10* resulted in pleiotropic developmental defects, reduced cell expansion, and hypersensitivity to salt stresses, similar to those caused by the functional loss of tonoplast proteins (Cheng et al., 2005; Krebs et al., 2010; Bassil et al., 2011b; Barragán et al., 2012). *pat10* also displayed a spectrum of reproductive defects, including sporophytic male and female defects as well as compromised growth of pollen tubes (Figures 2 to 4). The highly dynamic tubular vacuoles of pollen tubes (Hicks et al., 2004) may play critical roles in pollen germination and tube growth because disrupting vacuolar protein sorting often resulted in reduced pollen germination and poor male gametophytic transmission (Wang et al., 2010). Little is known about vacuole function in reproductive

tissues or cells. However, it is clear that male and female sporophytic cells undergo extensive secretion for the maturation of pollen (tapetal cells) or to support pollen tube growth (the transmitting tract), whereas genetically or pharmacologically interfering with vacuole function can disrupt both endocytic and secretory trafficking (Dettmer et al., 2006; Rojo and Denecke, 2008). Another possibility is that ion homeostasis regulated by vacuoles, as indicated by studies of tonoplast proteins (Cheng et al., 2005; Bassil et al., 2011b; Barragán et al., 2012; Tang et al., 2012), was disrupted in *pat10*, leading to the pleiotropic reproductive defects. It was shown that several animal PATs could act as cation transporters (Goytain et al., 2008; Hines et al., 2010); we therefore could not exclude the possibility that PAT10 plays similar roles directly rather than through its substrates.

Not all DHHC-type PATs identified so far show palmitate transferase activity (Ohno et al., 2012). However, the C192S mutation could not rescue *pat10* mutants, despite the fact that the majority of the mutant protein remained at the tonoplast (see Supplemental Figure 8 online), suggesting that PAT10 functions through its PAT activity. Therefore, we propose that PAT10 catalyzes the palmitoylation of proteins peripheral or integral to the tonoplast and thereby mediates vacuole function. Indeed, a similar regulatory paradigm occurred early during evolution. Pfa3, one of the seven DHHCs in yeast, catalyzes palmitoylation of Vac8, whose association with vacuolar membrane is critical for vacuolar trafficking and fusion (Hou et al., 2005; Smotrys et al., 2005).

Substrates of *Arabidopsis* PAT10

Our study suggests that tonoplast-localized CBL2/3/6 are putative substrates of PAT10. First, tonoplast-localized CBL2 is modified by palmitoylation, and mutating its potential palmitoylation sites rendered the protein cytosolic (Batistič et al., 2012). The Cys residues for palmitoylation were conserved for CBL3 and CBL6. Second, localization of CBL2 and CBL6 at the tonoplast did not rely on vesicle trafficking (Bottanelli et al., 2011; Batistič et al., 2012), suggesting that their palmitoylation was conducted by tonoplast-localized PATs. Third, we showed here that tonoplast localization of CBL2/3/6 was abolished by 2-BP treatment as well as in *pat10*. Because transient expression of *PAT10* resulted in mistargeting of PAT10 to the Golgi apparatus (Batistic, 2012), we could not test the effects of exogenous *PAT10* on the localization of CBLs in *pat10* nor the in planta interaction between PAT10 and CBL2/3/6.

More proteins are likely subjected to PAT10-mediated palmitoylation. First, *pat10* displayed pleiotropic developmental defects in the absence of abiotic stresses, which were not observed in loss-of-function mutants of *CBLs* (Batistic et al., 2010), although *cbl2 cbl3* double mutants showed pleiotropic defects, including leaf tip necrosis and reproductive defects (Tang et al., 2012). Second, although the *Arabidopsis* genome encodes other 21 PATs sharing the same domain organization with PAT10 (Hemsley et al., 2005; Hemsley and Grierson, 2008; Batistic, 2012), PAT10 is one of the only two PATs detected at the tonoplast (Batistic, 2012), suggesting low functional redundancy.

Global analysis of protein palmitoylation in yeast (Roth et al., 2006), in rat neuron (Kang et al., 2008), and in *Arabidopsis* (Hemsley et al., 2013) indicated that a large number of proteins are modified by palmitoylation, although this has yet to be shown experimentally. Because of the lack of consensus sequence for protein palmitoylation, it is impossible to perform an in silico prediction to evaluate the likely substrates of palmitoylation. Based on the subcellular localization and phenotypes of loss-of-function mutants, we consider some vacuolar transporters likely to be the substrates of PAT10, such as *Arabidopsis* NHX1 and NHX2 (Apse et al., 2003; Bassil et al., 2011a, 2011b; Barragán et al., 2012). Double mutants of *NHX1* and *NHX2* showed a spectrum of developmental and cellular defects (Bassil et al., 2011b) similar to those of *pat10*.

Palmitoylation may regulate the activities of transmembrane proteins, protein sorting, or protein–protein interaction. Unlike peripheral membrane proteins that will become cytosolic in the absence of their corresponding PATs, transmembrane proteins are membrane localized irrespective of palmitoylation. Perhaps for these reasons, only the receptor-like kinase FLAGELLIN SENSITIVE2 was experimentally shown to be regulated by palmitoylation, although many other receptor-like kinases as well as transporters were identified as putatively palmitoylated (Hemsley et al., 2013). Future technological improvements should help lead to the identification of transmembrane substrates of PAT10 at the tonoplast.

Subcellular Targeting of PAT10

PATs are multispan transmembrane proteins whose catalytic activities occur at or close to the membranes in which they reside (Hou et al., 2009). Therefore, there must be stringent mechanisms regulating their subcellular targeting to their final destination compartments. Although PATs of a given species can localize at diverse membrane compartments (Ohno et al., 2006; Greaves and Chamberlain, 2011; Batistic, 2012), little is known about the targeting determinants. Mutation at a palmitoyltransferase conserved C terminus (PaCCT) motif of yeast Pfa3 resulted in its functional loss and mistargeting to the vacuolar lumen (González Montoro et al., 2009). However, the PaCCT motif is not present in *Arabidopsis* PAT10.

35S-driven transient expression of *PAT10* showed a strong signal at the Golgi apparatus (Batistic, 2012), but such results could not be confirmed by in vivo approaches. We showed that the translational fusion of GFP at the C terminus of PAT10 functionally rescued *pat10* (see Supplemental Figure 6 online), thus allowing the analysis of its subcellular localization by fluorescence microscopy. Although transmembrane proteins are usually synthesized at the endoplasmic reticulum and delivered to their final destinations via vesicular trafficking, pharmacological treatments, together with fluorescent colabeling, showed that no PAT10 signal was detected at either the TGN/EE or the Golgi (see Supplemental Figure 9 online) upon BFA treatment, suggesting that PAT10 is transported to the vacuole through a route independent of the Golgi. We noticed that the C192S mutation resulted in partial translocation of PAT10 to the Golgi (see Supplemental Figure 10 online). It is known that the Cys residue within the DHHC motif is not only critical for PAT activity but is also itself a palmitoylation site (Greaves and Chamberlain, 2011). Therefore, the mislocalization caused by the C192S mutation could be due to interfered trafficking of PAT10, as $PAT10_{C192S}$ is not completely retained at the tonoplast. Because the functionality

of PATs is determined by their membrane localization, future efforts should be dedicated to verify the results obtained from a transient heterogeneous study (Batistic, 2012) using various in vivo approaches.

METHODS

Plant Materials and Growth Conditions

The *Arabidopsis thaliana* WAVE lines expressing RFP fusions for the TGN (WAVE2R), Golgi (WAVE22R), prevacuolar compartment (WAVE3R), and the tonoplast (WAVE9R) (Geldner et al., 2009) were obtained from the European Arabidopsis Stock Center (http://Arabidopsis.info). The T-DNA insertion lines SALK_024964 (*pat10-1*) and WiscDsLox289_292E10 (*pat10-2*) were obtained from the ABRC (http://www.Arabidopsis.org). The Columbia-0 ecotype was used as the wild type. *Arabidopsis* plants were grown in a 4:1:1 mix of Fafard 4P:perlite:vermiculite under an 18-h-light/6-h-dark cycle at 21°C. For growth on plates, surface-sterilized *Arabidopsis* seeds were placed on half-strength Murashige and Skoog (MS) basal medium with vitamins (Phytotechlab) except where noted. Plates were kept at 4°C in darkness for 4 d before being transferred to a growth chamber with a 16-h-light/8-h-dark cycle at 21°C. Stable *Arabidopsis* transformations were produced using the floral dipping method (Clough and Bent, 1998). Transgenic plants were selected on half-strength MS medium supplemented with 30 μg/mL Basta salt (Sigma-Aldrich). Measurement of epidermal cell sizes in mature leaves was performed as described (Ohto et al., 2005).

PCR, RT-PCR, and qRT-PCR

The segregation ratios in the reciprocal analysis were determined by PCR using the following primers: G1/G2 for *PAT10*, G3/G2 for *pat10-1*, G1/G4 for *PAT10*, and G5/G4 for *pat10-2*.

Total RNAs were isolated using a Qiagen RNeasy plant mini kit according to the manufacturer's instructions. Oligo(dT)-primed cDNAs were synthesized using Superscript III reverse transcriptase with on-column DNase digestion (Invitrogen). Primers used in RT-PCR to characterize *pat10* were R1/R2/R3/R4. Primers used in RT-PCR to verify complementation were R5/R6 for the endogenous *PAT10* and R5/R7 for the exogenous *PAT10*. Primers to amplify *ACTIN2* were as described (Zhang and McCormick, 2007).

The qRT-PCR analysis of salt-induced gene expression was performed with the Bio-Rad CFX96 real-time system using SYBR Green real-time PCR master mix (Toyobo). Each 20-μL reaction system contained 2 μL SYBR Green real-time PCR master mix, 2 μL cDNA, and 2 μL primers (5 μM). *GAPDH* and *TUBLIN2* were used as internal controls (Ryu et al., 2010). Primers used for *RD29A*, *RD20*, *ERD20*, *RAB18*, *GAPDH*, and *TUBLIN2* were as described (Ryu et al., 2010; Jiang et al., 2011). The cycling conditions were as followed: 95°C for 2 min and 42 cycles of 95°C for 15 s, 58°C for 15 s, and 72°C for 15 s. Fluorescence data were collected during the 72°C step and analyzed with the Bio-Rad CFX Manager. RNA extractions were performed for three biological replicates for each treatment, and three technical replicates were performed for each sample. The data presented in Figure 8 are means of the three biological replicates for which three technical replicates were averaged. All primers used in this study are listed in Supplemental Table 1 online.

Plasmid Construction

All constructs were generated using Gateway technology (Invitrogen). The whole genomic fragment of *PAT10* was cloned with primers PAT10gF/PAT10gR from genomic DNA. The C192S mutation was generated with primers PAT10gmF/PAT10gmR from the *PAT10g* entry vector using a Phusion site-directed mutagenesis kit according to the manufacturer's instructions (Finnzyme). The 1242-bp sequence upstream of the start codon of *PAT10* was used as its promoter (Pro_{PAT10}). Pro_{PAT10} was cloned with primers ProF/ProR from genomic DNA. The entry vectors for CBL2, CBL3, CBL6, CBL9, and ERD2 were generated from a mixed *Arabidopsis* cDNA library using the following primer pairs: CBL2-F/R for CBL2, CBL3-F/R for CBL3, CBL6-F/R for CBL6, CBL9-F/R for CBL9, and ERD2-F/R for ERD2. All entry clones were generated in the pENTR/D/TOPO vector (Invitrogen).

The destination vector used to generate Pro_{PAT10}:GUS were described previously (Curtis and Grossniklaus, 2003). The destination vector for *PAT10-GFP* and $PAT10_{C192S}$-*GFP* was modified from a previously described vector (Zhang and McCormick, 2007) by removing the Pro_{LAT52} sequence. The expression vector for ARA6 and ARA7 was described (Zhang et al., 2010). Expression vectors were generated by LR reactions using LR Clonase II (Invitrogen). Expression vectors for mbSUS were generated by in vivo homologous recombination in yeast as described (Obrdlik et al., 2004).

All PCR amplifications used Phusion hot start high-fidelity DNA polymerase with the annealing temperature and extension times recommended by the manufacturer (Finnzyme). All entry vectors were sequenced, and sequences were analyzed using Vector NTI (Invitrogen). The Bioneer PCR purification kit and Bioneer Spin miniprep kit were used for PCR product recovery and plasmid DNA extraction, respectively.

GUS Histochemistry

Roots of Pro_{PAT10}:GUS transgenic plants were fixed, cleared, and embedded in paraffin (Sigma-Aldrich). Fifteen embedded root tissues from three individual transgenic lines were analyzed. To show the outlines of cells, sectioned samples on slides were stained with 100 mg/L ruthenium red (Sigma-Aldrich) for 3 to 5 min before being visualized and photographed with an Olympus BX51 microscope equipped with a charge-coupled device camera.

RNA in Situ Hybridization

RNA in situ hybridization was performed as previously described (Li et al., 2010). Briefly, open flowers and young pistils were fixed in formaldehyde solution (formalin:acetic acid:ethanol:H_2O=1:2:10:7) overnight at 4°C, embedded in Paraplast (Sigma-Aldrich) after dehydration, and sectioned at 6-μm thickness. A 216-bp fragment specific for *PAT10* was amplified from the coding region of *PAT10* with primers ProbeF/ProbeR. The sense probe and the antisense probe were cloned into pMD19 T-simple vector (Takara), modified in vitro with digoxigenin-UTP by SP6 or T7 RNA polymerases (Roche), respectively. Sections were hybridized with 1.5 ng/μL probes at 42°C overnight in a hybridization solution that contained 50% formamide. Hybridization signals were detected using antidigoxigenin antibody (Anti-Digoxigenin-Ap Fab fragments; Roche). The samples were observed using an Olympus BX51 microscope.

Pollen Analysis

To detect pollen viability, mature anthers were soaked overnight in Alexander stain (Johnson-Brousseau and McCormick, 2004) and observed with a BX51 microscope (Olympus). Pollen from open flowers was stained with 1 mg/mL (w/v) 4',6-diamidino-2-phenylindole (Sigma-Aldrich) for 30 min and observed with an Axio Observer D1 microscope (Zeiss). Pollen germination in vitro and aniline blue staining of pollen tubes growing in vivo were performed as described (Zhang et al., 2009). For pollen SEM, mature pollen coated with gold palladium was observed under a JSM-6610LV scanning electron microscope (JEOL). For pollen TEM, mature flowers were fixed in 4% (v/v) glutaraldehyde and 1% (w/v) osmic acid

(Sigma-Aldrich). After washing with a phosphate buffer, the specimens were dehydrated in an ethanol series and embedded in Epon 812 resin (SPI-CHEM). Ultrathin sections were stained with acetate uranium and lead citrate. The specimens were observed using a JEM-1200EX transmission electron microscope (JEOL).

Pharmacological Treatment

For double labeling experiments with FM4-64, roots of 4- to 5-DAG seedlings were dipped in liquid MS media supplemented with 4 μM FM4-64 for 5 min (except for the 1-min assay). The roots were then taken out, washed three times with liquid MS medium without FM4-64, and visualized for FM4-64 intake at the designated times. For BFA treatment, roots were treated first with FM4-64 for 5 min, then washed and incubated with MS medium supplemented with 50 μM BFA for 50 min and visualized for the formation of BFA compartments. For treatment of protoplasts with 2-BP, 2-BP at the final concentration of 10 μM was added into cultural medium immediately after polyethylene glycol–mediated transformation. Samples were examined between 16 and 24 h after treatment.

Salt Treatment

For salt treatment, wild-type and *pat10* seedlings at 4 DAG on MS media were transferred to fresh MS media or to MS media supplemented with either 10 mM LiCl or 130 mM NaCl for additional 14 d. Plates were photographed with a BX51 microscope (Olympus) equipped with a digital camera. Rosette diameter was measured using ImageJ (http://rsbweb.nih.gov/ij/). For each treatment, a representative image from three independent experiments was shown. For the measurement of rosette diameter and fresh weight, each treatment was repeated three times, and each experiment included at least 30 plants from each genetic background.

For salt induction of gene expression, wild-type and *pat10* seedlings growing vertically on MS medium for 7 d were transferred to 3M filter paper presoaked with either MS medium or MS medium supplemented with 300 mM NaCl. After 6 h of incubation, whole seedlings were used for RNA extraction.

Expression in *Arabidopsis* Protoplasts

Preparation of *Arabidopsis* protoplasts was performed according to a previous report (Wu et al., 2009). Transformation of *Arabidopsis* protoplasts was performed according to standard protocols (Yoo et al., 2007). Three independent experiments for each treatment or combination were conducted to ensure that the results were consistent.

Fluorescent and Confocal Microscopy

In vitro growing pollen from *PAT10*-GFP or *PAT10*$_{C192S}$-GFP transgenic plants was captured by epifluorescence using Axio Observer D1 equipped with a charge-coupled device camera (Zeiss). Other images were captured by an inverted laser scanning confocal microscope (LSM780; Zeiss) with a Plan-Neofluar ×40/1.3 oil differential interference contrast objective or ×63/1.45 oil differential interference contrast objective. GFP-RFP double-labeled materials were captured alternately using line switching with the multitrack function (488 nm for GFP and 545 nm for RFP). Fluorescence was detected using a 505- to 550-nm band-pass filter for GFP and a 575- to 650-nm band-pass filter for RFP. Postacquisition image processing was performed with LSM image processing software (Zeiss). Pearson coefficients analysis was performed as described (French et al., 2008).

Optical sectioning of ovules was performed as described (Shi et al., 2005). Briefly, pistils were fixed in 4% glutaraldehyde (in 12.5 mM phosphate buffer, pH 6.9) for at least 20 min with vacuum and overnight at room temperature. After fixation, the tissues were dehydrated through a conventional ethanol series and cleared in 2:1 (v/v) benzyl benzoate: benzyl alcohol for at least 1 h. The pistils were then dissected, mounted with immersion oil, and observed with a Leica TCS SP5II laser scanning microscope (Leica) with a 488-nm argon laser and an LP 500 filter.

Accession Numbers

Sequence data from this article can be found in The Arabidopsis Information Resource database (www.Arabidopsis.org) under the following accession numbers: *PAT10* (At3g51390), *CBL2* (AT5G55990), *CBL3* (AT4G26570), *CBL6* (AT4G16350), *CBL9* (AT5G47100), *ARA6* (At3g54840), *ARA7* (AT4G19640), *ERD2* (AT1G29330), *RD29A* (AT5G52310), *RD20* (AT2G33380), *ERD10* (AT1G20450), *RAB18* (AT5G66400), *GAPDH* (AT3G04120), and *TUBLIN2* (AT5G62690).

Supplemental Data

The following materials are available in the online version of this article.

Supplemental Figure 1. Cell Size and Number Were Both Reduced in *pat10*.

Supplemental Figure 2. *PAT10* Mutations Caused Temporally Delayed but Developmentally Early Floral Transition.

Supplemental Figure 3. Pollen Viability Was Not Affected by *PAT10* Mutations.

Supplemental Figure 4. Embryo Sac Was Normal in Ovules from Heterozygous *pat10* Mutants.

Supplemental Figure 5. The Probe Used in RNA in Situ Hybridization Was Specific for *PAT10*.

Supplemental Figure 6. *PAT10*-GFP Complemented *pat10*.

Supplemental Figure 7. Subcellular Localization of PAT10 and PAT10$_{C192S}$ in Transgenic *Arabidopsis* Pollen Tubes Growing in Vitro.

Supplemental Figure 8. *PAT10*$_{C192S}$-GFP Did Not Complement *pat10*.

Supplemental Figure 9. PAT10 Localizes at the Tonoplast.

Supplemental Figure 10. PAT10$_{C192S}$ Localizes at the Tonoplast as well as BFA-Sensitive Vesicles.

Supplemental Figure 11. Treatment with 2-Bromopalmitate Abolished the Membrane Association of CBL2, CBL3, CBL6, and CBL9 in Wild-Type Protoplasts.

Supplemental Figure 12. Membrane Association of CBL9, ARA6, ARA7, and ERD2 Did Not Rely on Functional *PAT10*.

Supplemental Table 1. Primers Used in This Study.

ACKNOWLEDGMENTS

We thank the ABRC and European Arabidopsis Stock Center for the plant materials described in this article. We thank Xian Sheng Zhang for giving us access to the microscope facilities of his laboratory. This research was supported by Major Research Plan (2013CB945102) from the Ministry of Science and Technology of China and by a grant from the National Science Foundation of China (NSFC) (31261160490). Y.Z.'s laboratory is supported by the Tai-Shan Scholar program from Shandong Provincial Government. L.J. is supported by the Research Grants Council of Hong Kong and NSFC/RGC (N_CUHK406/12).

AUTHOR CONTRIBUTIONS

L.-Z.Z., S.L., Q.-N.F., Y.-L.Z. (SDAU), X.Z., Y.-L. Z. (CUHK), and H.W. performed the experiments. L.J. provided materials and helped with

microscopy. Y.Z. and S.L. designed the experiments and wrote the article.

Received December 21, 2012; revised February 11, 2013; accepted February 17, 2013; published March 12, 2013.

REFERENCES

Agee, A.E., et al. (2010). MODIFIED VACUOLE PHENOTYPE1 is an *Arabidopsis* myrosinase-associated protein involved in endomembrane protein trafficking. Plant Physiol. **152:** 120–132.

Apse, M.P., Sottosanto, J.B., and Blumwald, E. (2003). Vacuolar cation/H^+ exchange, ion homeostasis, and leaf development are altered in a T-DNA insertional mutant of *AtNHX1*, the *Arabidopsis* vacuolar Na^+/H^+ antiporter. Plant J. **36:** 229–239.

Baekkeskov, S., and Kanaani, J. (2009). Palmitoylation cycles and regulation of protein function (Review). Mol. Membr. Biol. **26:** 42–54.

Barragán, V., Leidi, E.O., Andrés, Z., Rubio, L., De Luca, A., Fernández, J.A., Cubero, B., and Pardo, J.M. (2012). Ion exchangers NHX1 and NHX2 mediate active potassium uptake into vacuoles to regulate cell turgor and stomatal function in *Arabidopsis*. Plant Cell **24:** 1127–1142.

Bassil, E., Ohto, M.A., Esumi, T., Tajima, H., Zhu, Z., Cagnac, O., Belmonte, M., Peleg, Z., Yamaguchi, T., and Blumwald, E. (2011a). The *Arabidopsis* intracellular Na^+/H^+ antiporters NHX5 and NHX6 are endosome associated and necessary for plant growth and development. Plant Cell **23:** 224–239.

Bassil, E., Tajima, H., Liang, Y.C., Ohto, M.A., Ushijima, K., Nakano, R., Esumi, T., Coku, A., Belmonte, M., and Blumwald, E. (2011b). The *Arabidopsis* Na^+/H^+ antiporters NHX1 and NHX2 control vacuolar pH and K^+ homeostasis to regulate growth, flower development, and reproduction. Plant Cell **23:** 3482–3497.

Batistic, O. (2012). Genomics and localization of the *Arabidopsis* DHHC-cysteine-rich domain S-acyltransferase protein family. Plant Physiol. **160:** 1597–1612.

Batistic, O., and Kudla, J. (2009). Plant calcineurin B-like proteins and their interacting protein kinases. Biochim. Biophys. Acta **1793:** 985–992.

Batistič, O., Rehers, M., Akerman, A., Schlücking, K., Steinhorst, L., Yalovsky, S., and Kudla, J. (2012). S-acylation-dependent association of the calcium sensor CBL2 with the vacuolar membrane is essential for proper abscisic acid responses. Cell Res. **22:** 1155–1168.

Batistic, O., Sorek, N., Schültke, S., Yalovsky, S., and Kudla, J. (2008). Dual fatty acyl modification determines the localization and plasma membrane targeting of CBL/CIPK Ca^{2+} signaling complexes in *Arabidopsis*. Plant Cell **20:** 1346–1362.

Batistic, O., Waadt, R., Steinhorst, L., Held, K., and Kudla, J. (2010). CBL-mediated targeting of CIPKs facilitates the decoding of calcium signals emanating from distinct cellular stores. Plant J. **61:** 211–222.

Bottanelli, F., Foresti, O., Hanton, S., and Denecke, J. (2011). Vacuolar transport in tobacco leaf epidermis cells involves a single route for soluble cargo and multiple routes for membrane cargo. Plant Cell **23:** 3007–3025.

Cheng, N.H., Pittman, J.K., Shigaki, T., Lachmansingh, J., LeClere, S., Lahner, B., Salt, D.E., and Hirschi, K.D. (2005). Functional association of *Arabidopsis* CAX1 and CAX3 is required for normal growth and ion homeostasis. Plant Physiol. **138:** 2048–2060.

Cheung, A.Y., Chen, C.Y., Glaven, R.H., de Graaf, B.H.J., Vidali, L., Hepler, P.K., and Wu, H.M. (2002). Rab2 GTPase regulates vesicle trafficking between the endoplasmic reticulum and the Golgi bodies and is important to pollen tube growth. Plant Cell **14:** 945–962.

Clough, S.J., and Bent, A.F. (1998). Floral dip: A simplified method for *Agrobacterium*-mediated transformation of *Arabidopsis thaliana*. Plant J. **16:** 735–743.

Curtis, M.D., and Grossniklaus, U. (2003). A gateway cloning vector set for high-throughput functional analysis of genes in planta. Plant Physiol. **133:** 462–469.

Dettmer, J., Hong-Hermesdorf, A., Stierhof, Y.D., and Schumacher, K. (2006). Vacuolar H^+-ATPase activity is required for endocytic and secretory trafficking in *Arabidopsis*. Plant Cell **18:** 715–730.

Ebine, K., et al. (2011). A membrane trafficking pathway regulated by the plant-specific RAB GTPase ARA6. Nat. Cell Biol. **13:** 853–859.

French, A.P., Mills, S., Swarup, R., Bennett, M.J., and Pridmore, T.P. (2008). Colocalization of fluorescent markers in confocal microscope images of plant cells. Nat. Protoc. **3:** 619–628.

Gagne, J.M., and Clark, S.E. (2010). The *Arabidopsis* stem cell factor POLTERGEIST is membrane localized and phospholipid stimulated. Plant Cell **22:** 729–743.

Geldner, N., Dénervaud-Tendon, V., Hyman, D.L., Mayer, U., Stierhof, Y.D., and Chory, J. (2009). Rapid, combinatorial analysis of membrane compartments in intact plants with a multicolor marker set. Plant J. **59:** 169–178.

González Montoro, A., Quiroga, R., Maccioni, H.J., and Valdez Taubas, J. (2009). A novel motif at the C-terminus of palmitoyltransferases is essential for Swf1 and Pfa3 function *in vivo*. Biochem. J. **419:** 301–308.

Goytain, A., Hines, R.M., and Quamme, G.A. (2008). Huntingtin-interacting proteins, HIP14 and HIP14L, mediate dual functions, palmitoyl acyltransferase and Mg^{2+} transport. J. Biol. Chem. **283:** 33365–33374.

Greaves, J., and Chamberlain, L.H. (2011). DHHC palmitoyl transferases: Substrate interactions and (patho)physiology. Trends Biochem. Sci. **36:** 245–253.

Hamaji, K., et al. (2009). Dynamic aspects of ion accumulation by vesicle traffic under salt stress in *Arabidopsis*. Plant Cell Physiol. **50:** 2023–2033.

Hemsley, P.A., and Grierson, C.S. (2008). Multiple roles for protein palmitoylation in plants. Trends Plant Sci. **13:** 295–302.

Hemsley, P.A., Kemp, A.C., and Grierson, C.S. (2005). The TIP GROWTH DEFECTIVE1 S-acyl transferase regulates plant cell growth in *Arabidopsis*. Plant Cell **17:** 2554–2563.

Hemsley, P.A., Weimar, T., Lilley, K.S., Dupree, P., and Grierson, C.S. (2013). A proteomic approach identifies many novel palmitoylated proteins in *Arabidopsis*. New Phytol. **197:** 805–814.

Hicks, G.R., Rojo, E., Hong, S., Carter, D.G., and Raikhel, N.V. (2004). Geminating pollen has tubular vacuoles, displays highly dynamic vacuole biogenesis, and requires *VACUOLESS1* for proper function. Plant Physiol. **134:** 1227–1239.

Hines, R.M., Kang, R., Goytain, A., and Quamme, G.A. (2010). Golgi-specific DHHC zinc finger protein GODZ mediates membrane Ca^{2+} transport. J. Biol. Chem. **285:** 4621–4628.

Hou, H., John Peter, A.T., Meiringer, C., Subramanian, K., and Ungermann, C. (2009). Analysis of DHHC acyltransferases implies overlapping substrate specificity and a two-step reaction mechanism. Traffic **10:** 1061–1073.

Hou, H., Subramanian, K., LaGrassa, T.J., Markgraf, D., Dietrich, L.E., Urban, J., Decker, N., and Ungermann, C. (2005). The DHHC protein Pfa3 affects vacuole-associated palmitoylation of the fusion factor Vac8. Proc. Natl. Acad. Sci. USA **102:** 17366–17371.

Jiang, T., Zhang, X.F., Wang, X.F., and Zhang, D.P. (2011). *Arabidopsis* 3-ketoacyl-CoA thiolase-2 (KAT2), an enzyme of fatty acid β-oxidation, is involved in ABA signal transduction. Plant Cell Physiol. **52:** 528–538.

Johnson-Brousseau, S.A., and McCormick, S. (2004). A compendium of methods useful for characterizing *Arabidopsis* pollen mutants and gametophytically-expressed genes. Plant J. **39:** 761–775.

Kang, R., et al. (2008). Neural palmitoyl-proteomics reveals dynamic synaptic palmitoylation. Nature **456:** 904–909.

Kim, B.-G., Waadt, R., Cheong, Y.H., Pandey, G.K., Dominguez-Solis, J.R., Schültke, S., Lee, S.C., Kudla, J., and Luan, S. (2007). The calcium sensor CBL10 mediates salt tolerance by regulating ion homeostasis in *Arabidopsis*. Plant J. **52:** 473–484.

Kim, S.J., and Bassham, D.C. (2011). TNO1 is involved in salt tolerance and vacuolar trafficking in *Arabidopsis*. Plant Physiol. **156:** 514–526.

Krebs, M., Beyhl, D., Görlich, E., Al-Rasheid, K.A., Marten, I., Stierhof, Y.D., Hedrich, R., and Schumacher, K. (2010). *Arabidopsis* V-ATPase activity at the tonoplast is required for efficient nutrient storage but not for sodium accumulation. Proc. Natl. Acad. Sci. USA **107:** 3251–3256.

Lam, S.K., Cai, Y., Tse, Y.C., Wang, J., Law, A.H., Pimpl, P., Chan, H.Y., Xia, J., and Jiang, L. (2009). BFA-induced compartments from the Golgi apparatus and *trans*-Golgi network/early endosome are distinct in plant cells. Plant J. **60:** 865–881.

Lam, S.K., Siu, C.L., Hillmer, S., Jang, S., An, G., Robinson, D.G., and Jiang, L. (2007). Rice SCAMP1 defines clathrin-coated, *trans*-golgi-located tubular-vesicular structures as an early endosome in tobacco BY-2 cells. Plant Cell **19:** 296–319.

Li, X.G., Su, Y.H., Zhao, X.Y., Li, W., Gao, X.Q., and Zhang, X.S. (2010). Cytokinin overproduction-caused alteration of flower development is partially mediated by *CUC2* and *CUC3* in *Arabidopsis*. Gene **450:** 109–120.

Luan, S. (2009). The CBL-CIPK network in plant calcium signaling. Trends Plant Sci. **14:** 37–42.

Maeshima, M. (2001). TONOPLAST TRANSPORTERS: Organization and function. Annu. Rev. Plant Physiol. Plant Mol. Biol. **52:** 469–497.

Magnan, F., Ranty, B., Charpenteau, M., Sotta, B., Galaud, J.P., and Aldon, D. (2008). Mutations in AtCML9, a calmodulin-like protein from *Arabidopsis thaliana*, alter plant responses to abiotic stress and abscisic acid. Plant J. **56:** 575–589.

Martín, M.L., and Busconi, L. (2000). Membrane localization of a rice calcium-dependent protein kinase (CDPK) is mediated by myristoylation and palmitoylation. Plant J. **24:** 429–435.

Mimura, T., Kura-Hotta, M., Tsujimura, T., Ohnishi, M., Miura, M., Okazaki, Y., Mimura, M., Maeshima, M., and Washitani-Nemoto, S. (2003). Rapid increase of vacuolar volume in response to salt stress. Planta **216:** 397–402.

Obrdlik, P., et al. (2004). K^+ channel interactions detected by a genetic system optimized for systematic studies of membrane protein interactions. Proc. Natl. Acad. Sci. USA **101:** 12242–12247.

Ohno, Y., Kihara, A., Sano, T., and Igarashi, Y. (2006). Intracellular localization and tissue-specific distribution of human and yeast DHHC cysteine-rich domain-containing proteins. Biochim. Biophys. Acta **1761:** 474–483.

Ohno, Y., Kashio, A., Ogata, R., Ishitomi, A., Yamazaki, Y., and Kihara, A. (2012). Analysis of substrate specificity of human DHHC protein acyltransferases using a yeast expression system. Mol. Biol. Cell **23:** 4543–4551.

Ohto, M.A., Fischer, R.L., Goldberg, R.B., Nakamura, K., and Harada, J.J. (2005). Control of seed mass by APETALA2. Proc. Natl. Acad. Sci. USA **102:** 3123–3128.

Pandey, G.K., Cheong, Y.H., Kim, K.N., Grant, J.J., Li, L., Hung, W., D'Angelo, C., Weinl, S., Kudla, J., and Luan, S. (2004). The calcium sensor calcineurin B-like 9 modulates abscisic acid sensitivity and biosynthesis in *Arabidopsis*. Plant Cell **16:** 1912–1924.

Pittman, J.K. (2011). Vacuolar $Ca^{(2+)}$ uptake. Cell Calcium **50:** 139–146.

Rojo, E., and Denecke, J. (2008). What is moving in the secretory pathway of plants? Plant Physiol. **147:** 1493–1503.

Roth, A.F., Wan, J., Bailey, A.O., Sun, B., Kuchar, J.A., Green, W.N., Phinney, B.S., Yates, J.R., and III., Davis, N.G. (2006). Global analysis of protein palmitoylation in yeast. Cell **125:** 1003–1013.

Ryu, M.Y., Cho, S.K., and Kim, W.T. (2010). The *Arabidopsis* C3H2C3-type RING E3 ubiquitin ligase AtAIRP1 is a positive regulator of an abscisic acid-dependent response to drought stress. Plant Physiol. **154:** 1983–1997.

Shi, D.Q., Liu, J., Xiang, Y.H., Ye, D., Sundaresan, V., and Yang, W.C. (2005). *SLOW WALKER1*, essential for gametogenesis in *Arabidopsis*, encodes a WD40 protein involved in 18S ribosomal RNA biogenesis. Plant Cell **17:** 2340–2354.

Smotrys, J.E., Schoenfish, M.J., Stutz, M.A., and Linder, M.E. (2005). The vacuolar DHHC-CRD protein Pfa3p is a protein acyltransferase for Vac8p. J. Cell Biol. **170:** 1091–1099.

Sorek, N., Poraty, L., Sternberg, H., Bar, E., Lewinsohn, E., and Yalovsky, S. (2007). Activation status-coupled transient S acylation determines membrane partitioning of a plant Rho-related GTPase. Mol. Cell. Biol. **27:** 2144–2154.

Sorek, N., Segev, O., Gutman, O., Bar, E., Richter, S., Poraty, L., Hirsch, J.A., Henis, Y.I., Lewinsohn, E., Jürgens, G., and Yalovsky, S. (2010). An S-acylation switch of conserved G domain cysteines is required for polarity signaling by ROP GTPases. Curr. Biol. **20:** 914–920.

Tang, R.-J., Liu, H., Yang, Y., Yang, L., Gao, X.-S., Garcia, V.J., Luan, S., and Zhang, H.-X. (2012). Tonoplast calcium sensors CBL2 and CBL3 control plant growth and ion homeostasis through regulating V-ATPase activity in *Arabidopsis*. Cell Res. **22:** 1650–1665.

Ueda, T., Yamaguchi, M., Uchimiya, H., and Nakano, A. (2001). Ara6, a plant-unique novel type Rab GTPase, functions in the endocytic pathway of *Arabidopsis thaliana*. EMBO J. **20:** 4730–4741.

Wang, H., Tse, Y.C., Law, A.H., Sun, S.S., Sun, Y.B., Xu, Z.F., Hillmer, S., Robinson, D.G., and Jiang, L. (2010). Vacuolar sorting receptors (VSRs) and secretory carrier membrane proteins (SCAMPs) are essential for pollen tube growth. Plant J. **61:** 826–838.

Wu, F.-H., Shen, S.-C., Lee, L.-Y., Lee, S.-H., Chan, M.-T., and Lin, C.-S. (2009). Tape-*Arabidopsis* sandwich - A simpler *Arabidopsis* protoplast isolation method. Plant Methods **5:** 16.

Yoo, S.D., Cho, Y.H., and Sheen, J. (2007). *Arabidopsis* mesophyll protoplasts: A versatile cell system for transient gene expression analysis. Nat. Protoc. **2:** 1565–1572.

Zeng, Q., Wang, X., and Running, M.P. (2007). Dual lipid modification of *Arabidopsis* Ggamma-subunits is required for efficient plasma membrane targeting. Plant Physiol. **143:** 1119–1131.

Zhang, Y., He, J., Lee, D., and McCormick, S. (2010). Interdependence of endomembrane trafficking and actin dynamics during polarized growth of *Arabidopsis* pollen tubes. Plant Physiol. **152:** 2200–2210.

Zhang, Y., He, J., and McCormick, S. (2009). Two *Arabidopsis* AGC kinases are critical for the polarized growth of pollen tubes. Plant J. **58:** 474–484.

Zhang, Y., and McCormick, S. (2007). A distinct mechanism regulating a pollen-specific guanine nucleotide exchange factor for the small GTPase Rop in *Arabidopsis thaliana*. Proc. Natl. Acad. Sci. USA **104:** 18830–18835.

Zimmermann, P., Hirsch-Hoffmann, M., Hennig, L., and Gruissem, W. (2004). GENEVESTIGATOR. Arabidopsis microarray database and analysis toolbox. Plant Physiol. **136:** 2621–2632.